Bulletin of Electrical Engineering and Informatics
Vol. 10, No. 3, June 2021, pp. 1709~1717
ISSN: 2302-9285, DOI: 10.11591/eei.v10i3.3042

Employing SiO_2 nano-particles in conformal and in-cup structures of 8500 K white LEDs

My Hanh Nguyen Thi[1], Phung Ton That[2]
[1]Faculty of Mechanical Engineering, Industrial University of Ho Chi Minh City, Viet Nam
[2]Faculty of Electronics Technology, Industrial University of Ho Chi Minh City, Ho Chi Minh city, Vietnam

Article Info

Article history:

Received Dec 16, 2020
Revised Mar 2, 2021
Accepted May 4, 2021

Keywords:

Correlated color temperature
Mie-scattering theory
Phosphor structure
SiO_2 nano-particles

ABSTRACT

SiO_2 nano-particles have been examined in a distant phosphor structure for the elevated luminous quality and better consistency of white light-emitting diodes with angular-dependent associated color temperature (CCT). The luminous scattering ability could be increased by applying SiO_2 nano-particles contain silicone to the outside of the phosphorus coating. In specific, the strength of blue light at wide angles is increased and differences in CCT can be minimized. In addition, owing to the sufficient refractive indices of silicone-containing SiO_2 nanoparticles between the air and phosphorus layers, the luminous flux was improved. This new configuration decreases angular-dependent CCT deviations in the range of -70^0 to 70^0 from 1000 to 420 K. In comparison, at a 120 mA driving current, the rise of lumen flux increased by 2.25% relative to an usual distant phosphor structure without SiO_2 nano-particles. As a result, in a distant phosphor structure, the SiO_2 nano-particles could not only enhance the uniformity of illumination but also enhance the output of light.

Corresponding Author:

My Hanh Nguyen Thi
Faculty of Mechanical Engineering
Industrial University of Ho Chi Minh City
No. 12 Nguyen Van Bao Street, Ho Chi Minh City, Vietnam
Email: nguyenthimyhanh@iuh.edu.vn

1. INTRODUCTION

Light emitting diodes (LEDs) are utilized commonly such as replacements for frequently utilized incandescent bulbs and fluorescent lamps which are ineffective or include mercury [1]. Phosphors are normally added to blue light from LED chips that have down-conversion in order to recognize white light. Relied on the downshift of blue InGaN LEDs by $Y_3Al_5O_{12}$:Ce (YAG:Ce)-based yellow phosphors, white LEDs presently produce a "cold" white light with a poor color rendering index (CRI) and superior correlated color temperature (CCT). Phosphors have been pushed beyond the normal YAG: Ce. The demand to substitute incandescent lamps producing "warm" white color with a novel illumination supply with superior CRI and poor CCT has pushed phosphors outside the usual YAG: Ce. Mixing red emitted phosphors with yellow phosphors will enhance color intensity but capacity of the energy of LEDs will be remarkably reduced [2]. After that, among light output and white LED power efficiency there will be an exchange. Lately, as potential candidates for light emissions, semiconductor nanocrystals or quantum dots (QDs) have been introduced to adjust the emission spectrum of standard white LEDs that have the decreased reduction of capacity quality [3]. QDs are effective visible light emissions that provide extremely narrow emission spectrums with precisely adjustable wavelengths of emission. Thus, highly effective white LEDs which have superior CRI are predicted. However, QDs require a consistent combination of a silicone polymer in the

packing procedure of white LEDs and above ligands of QDs could potentially impede the polymerizing or decrease the mechanically stable of packing stuffs [4]. In addition, the appropriation with silicone polymers with polarization, which is liked better in LED manufacturing, is reduced by the long chain outside-covering ligands with the hydrophobicity. Ziegler et al. recommended silica-encapsulated QDs to resolve these difficulties and have a high CRI for increased LED emission spectrums. Nanocomposites which have the base of inorganic nanocrystals have been of great attentiveness in previous decades as the ability of them to control their physical and chemical features for diverse implementations like light-emitting diodes (LEDs), catalysts, creating biological images [5]-[9]. The most thoroughly studied of these are silica-based nanocomposites with quantum dots (QDs). Though many routes have been attempted to nanocomposites which have the base of silica with precisely scattered QDs, the process including a interchange stage of ligand as for the semiconductor nanocrystal hydrophilic outside-covering and following expansion using the Sto¨ber method of silica shell layer is one of the more common routes [10], [11]. Additionally, to synthesize SiO_2-nanocrystal composite particles, an opposite micelle technique was also commonly adopted [12]-[15]. In order to induce the production of reverse micelles, surfactants have been used and silica precursors (e.g. tetraethylorthosilicate, TEOS) are hydrolyzed/condensed at the interface of water and oil. With this method, a smug silica outside-covering was acquired because of the great monodispersity. Koole et al. recently indicated that hydrolyzed TEOS could substitute the water repellent ligands of the QD facade where silica development occurs. Although the amount of nanocrystals embedded in each nanocomposite particle is typically restricted, SiO_2 nanohybrids with numerous nanocrystals at great concentrations are used in the synthesis of greatly luminescent phosphors for many impementations [16].

2. EXPERIMENTAL DETAILS

2.1. MC-WLEDs simulation

An illustration of the structure of WLEDs is given in Figure 1. Samples with remote phosphorous formations are produced in the plastic lead-frame box in the following stages: (1) a square blue LED chips has the size of 24 mils and a greatest emission wavelength of 450 nm are mounted. The radiant flux of the pure blue LED chips of a moving current of 120 mA was 95 mW, (2) By dispensing, the translucent silicone is loaded in the lead frame and cured for 1 h at 1500C, (3) The phosphorus dusts are amalgamated with a silicone adhesive and a solvent has the base of alkyl in order to create phosphorus termination slurry. As previously shown, the pulsation spray covering with the time management could boost the phosphorous slurry quality [17], [18].

The phosphorous $Y_3Al_5O_{12}$ (YAG) is used with a particle size of around 12 μm in this experiment. The phosphorus slurry is then sprayed on the translucent silicone surface to form the usual distant phosphorus, Figure 1(a). The manufacture of nanoparticles of SiO_2 with distant phosphorous configuration varies only in the final stage from the usual distant phosphorous configuration, Figure 1(b). SiO_2 nano-particles are combined and sprayed on the surface of the phosphorous substrate with an alkyl-based solvent and a silicone adhesive, with a 5% concentration of SiO_2 nano-particles. The LED is chosen for contrast at a moving current of 120 mA which has the similar color temperature and color intensity coordinates. So as to examine the investigational consequence of SiO_2 nano-particles in the silicone sealant, the cross-sectional scanning electron microscopic (SEM) illustration is also used. It demonstrates the size of SiO_2 nano-particles at approximately 300 nm, Figure 1(c). An energy dispersive spectrometer (EDS) was examined for the portion of SiO_2 nano-particles with silicone encapsulant, as shown in Figure 1(d). In the silicone encapsulant, we can check the presence of Si and O components.

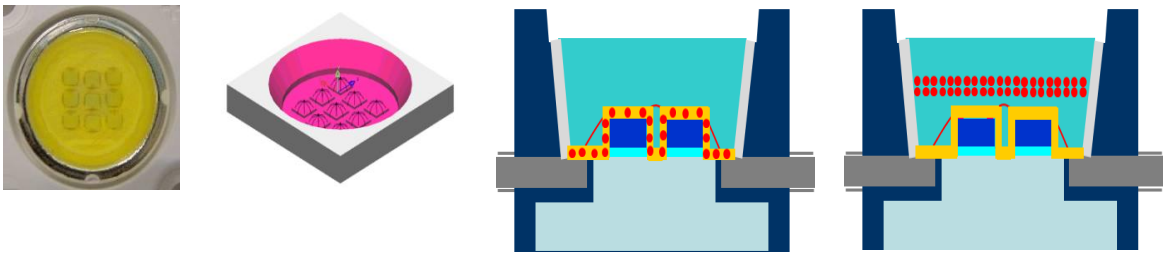

(a) (b) (c) (d)

Figure 1. These figures are, (a) Picture of WLEDs form, (b) The simulated WLEDs model, (c) Conformal phosphor structure, (d) In-cup phosphor structure

2.2. Scattering computation

The Mie theoretical [19]-[22] findings and the ray-tracing outcomes are farther debated as a possibility to figure out if the Mie theory could be updated by an uncomplicated approach to provide an extra detailed explanation of the optic characteristics of phosphorus. It is as Mie theory is commonly applied in a lot of mercantile optic softwares such as LightTools, Tracepro, and ASAP, which normally considers phosphor scattering to be Mie scattering to recognize the optic simulation of the packaging of white LED. Altered Mie optic constant calculations can give fair optical simulation assistance and help the software in a superior way in the LED packaging design. The scattering coefficient $\mu_{sca}(\lambda)$, anisotropy factor $g(\lambda)$, and declined scattering coefficient $\delta_{sca}(\lambda)$ could be calculated by the calcutions (1), (2), and (3) according to the Mie-scattering theory:

$$\mu_{sca}(\lambda) = \int N(r) C_{sca}(\lambda, r) dr \tag{1}$$

$$g(\lambda) = 2\pi \int_{-1}^{1} \int p(\theta, \lambda, r) f(r) \cos\theta d\cos\theta dr \tag{2}$$

$$\delta_{sca} = \mu_{sca}(1-g) \tag{3}$$

Where $N(r)$ shows diffusion particle distribution density (mm^3), C_{sca} is the diffusion cross-section (mm^2), $p(\theta,\lambda,r)$ is the phase function, λ is the luminous wavelength (nm), r is the diffusion particle radius (μm), θ is the scattering angle (°C), and $f(r)$ is the phosphorous layer diffuser distribution function, which can be computed as shown below [23], [24]:

$$f(r) = f_{dif}(r) + f_{phos}(r) \tag{4}$$

$$\begin{aligned} N(r) &= N_{dif}(r) + N_{phos}(r) \\ &= K_N.[f_{dif}(r) + f_{phos}(r)] \end{aligned} \tag{5}$$

The diffusive particle density $N_{dif}(r)$ and the phosphor particle density $N(r)$ consisting of $N_{phos}(r)$. $f_{dif}(r)$ and $f_{phos}(r)$ are the function data of the diffuser and the dimension dispensation of phosphor particle. K_N is the diffuser unit number for a single diffuser concentration and can be determined as below [25], [26]:

$$c = K_N \int M(r) dr \tag{6}$$

Where $M(r)$ is the diffusive unit's mass distribution, proposed by the equation [27]:

$$M(r) = \frac{4}{3}\pi r^3 [\rho_{dif} f_{dif}(r) + \rho_{phos} f_{phos}(r)] \tag{7}$$

$\rho_{diff}(r)$ and $\rho_{phos}(r)$ are the density of diffuser and phosphor crystal. According to Mie theory, C_{sca} could be acquired by the calculation below [28]:

$$C_{sca} = \frac{2\pi}{k^2} \sum_{0}^{\infty} (2n-1)(|a_n|^2 + |b_n|^2) \tag{8}$$

Where $k=2\pi/\lambda$, and a_n and b_n are computed as follows:

$$a_n(x,m) = \frac{\psi_n'(mx)\psi_n(x) - \mathrm{m}\psi_n(mx)\psi_n'(x)}{\psi_n'(mx)\xi_n(x) - \mathrm{m}\psi_n(mx)\xi_n'(x)} \tag{9}$$

$$b_n(x,m) = \frac{m\psi_n'(mx)\psi_n(x) - \psi_n(mx)\psi_n'(x)}{m\psi_n'(mx)\xi_n(x) - \psi_n(mx)\xi_n'(x)} \tag{10}$$

Where $x=k.r$, m is the refractive index, and $\psi_n(x)$ and $\xi_n(x)$ are the Riccati-Bessel function.

Therefore, the correlative refractive indices of diffusor (m_{dif}) and phosphor (m_{phos}) in silicone could be computed as $m_{dif} = n_{dif} / n_{sil}$ and $m_{phos} = n_{phos} / n_{sil}$. After that, the phase function could be shown as follows:

$$p(\theta,\lambda,r) = \frac{4\pi\beta(\theta,\lambda,r)}{k^2 C_{sca}(\lambda,r)} \tag{11}$$

Where $\beta(\theta,\lambda,r)$, $S_1(\theta)$ and $S_2(\theta)$ are the angular scatter amplitudes computed by the expressions below [29]:

$$\beta(\theta,\lambda,r) = \frac{1}{2}[|S_1(\theta)|^2 + |S_2(\theta)|^2] \tag{12}$$

$$S_1 = \sum_{n=1}^{\infty} \frac{2n+1}{n(n+1)} \begin{bmatrix} a_n(x,m)\pi_n(\cos\theta) \\ +b_n(x,m)\tau_n(\cos\theta) \end{bmatrix} \tag{13}$$

$$S_2 = \sum_{n=1}^{\infty} \frac{2n+1}{n(n+1)} \begin{bmatrix} a_n(x,m)\tau_n(\cos\theta) \\ +b_n(x,m)\pi_n(\cos\theta) \end{bmatrix} \tag{14}$$

Even though the optical characteristics of the YAG: Ce crystal have been thoroughly analyzed, due to the various amounts of Ce doping, crystal growth approaches, and measuring instruments, the α differs in a wide range. The α variation is usually in the blue light spectrum of 3-8mm^{-1}. However, for optical YAG:Ce ceramics, composed of little crystal grains, the absorptivity of light is notably increased and the α may be greater than 15 mm^{-1}. It is owing to the numerous reflections inside the grain, which enhance the whole luminous absorptivity. Provided that the phosphorus studied is the powder composed of crystals and may therefore have great α, this analysis sets alpha ranged from 8 to 20 mm^{-1} for the blue light to study the variants of C_{sca} (453). The estimated results of C_{sca} (453) are shown in Figure 2. According to (1), μ_{sca} is measured and shown in Figure 3. It can be shown in Figure 2 that one amplitude greater than the cross segment of absorption is the scattering cross segment, which means that the phosphorus has a powerful scatter impact and hence overcomes in great blue light absorptivity. With the rise of phosphorus concentration, the absorptivity and scatter coefficients are improved linearly in Figure 3, suggesting that changing the concentration of phosphorus is a direct response to white LED color control.

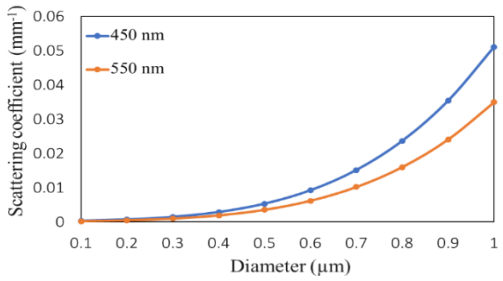

Figure 2. Scattering coefficients of SiO_2 particles

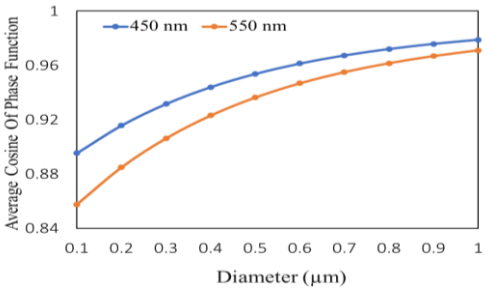

Figure 3. The phase function of SiO_2 particles

In the optic configuration of the measuring basis, light of blue or the light of yellow is generated from the above outside covering of the chip with a Lambertian pattern of radiation. The material for the lenses is Schott's BK7. The inside surfaces of the two merging spheres are covered with a diffuse white substance having optic characteristics of 11.1% absorptivity and 89.9% dispersion. The phosphor slide's help glass is also BK7 glass. In order to gather the emitted and reflected light, the surfaces inside the merging spheres are used as the receivers. For the ray tracing of the optical model, the Monte Carlo approach is applied. Phosphor is thought to be a material for dispersing Mie. Because the ray tracing is unable to measure the dispersion paths of the illumination in the phosphorus directly, the Henyey-Greenstein function is utilized as estimation for the angular dispersion generation, see Figure 3. We initially introduced the Mie theoretical results without any enhancement in the optic configuration. Nevertheless, the ray-tracing consequences

indicated that the transmission was slightly greater than that of the calculation overcomes and the absorptivity of the light of blue was lower than that of the calculation overcomes. These variations bring on three explanations. As compared with the real values, these are the lower μ_{abs}, lower μ_{sca}, and higher $g(\lambda)$. Therefore in the following simulations, three methodologies were introduced to achieve more accurate optical constants. The technique retained one of three constants unchanged in series and modified the other two constants to estimate the outcome of the experiment at the same time.

3. RESULTS AND DISCUSSION

Generally, the consistency that dependending on the angle of CCT could be described as the maximal CCT minus the minimal CCT. Diverse densities of SiO_2 nano-particles with a coating by silicone above the distant phosphorous formation are manufactured to advance the CCT aberration, Figure 4. This is evident that the littlest CCT aberrations and maximum density of SiO_2 nano-particles are seen at 10 mg cm^{-2}, which could achieve a 58% increase relative with the standard configuration of distant phosphorus. The inset illustration of Figure 4 illustrates the distant-field views of distant phosphor structures for normal and SiO_2 nano-particles. With the scattered function that SiO_2 nano-particles have, the light of blue and yellow can be evenly scattered. The CCT deviations will however be influenced by more SiO_2 nano-particles than 10 mg cm^2, but the quality is much higher than the conventional distant phosphorus configuration. The findings showed that the 10 mg cm^2 SiO_2 nano-particles' distant phosphorous configuration was not only able to boost the homogeneity of CCT that dependent on the angle, but also to enhance the flux of lumination.

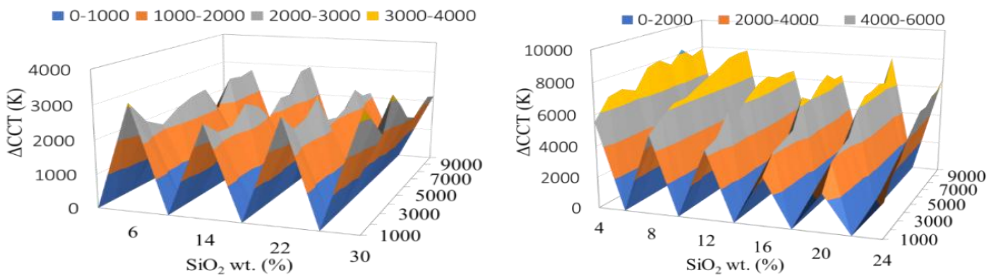

(a) (b)

Figure 4. CCT deviations of SiO_2 particles with different diameters, (a) Conformal structure, (b) In-cup geometry

The angular-dependent CCT of the distant phosphor structures of the normal and SiO_2 nano-particles is calculated and the SiO_2 layer weight is 10 mg cm^{-2}. Obviously, the angular-dependent CCT variance of the distant phosphorus structures of conventional and SiO_2 nano-particles has been increased from 1000 to 420 K in the scope of 700 to 700. The traditional distant phosphorus configuration has a lower angular CCT variance owing to the light of blue being limitted and mirrored in the phosphor cover at a wide angle. Therefore, wide-angle extraction of blue light is minimized, leading to inefficient color blending of the light of blue and yellow. SiO_2 nanoparticles have a finer silicone angular-dependent CCT distribution on the phosphorous layer surface, as SiO_2 nano-particles may have an effective dispersion possibility to enhance the scale of the light of yellow to the light of blue at wide angles. Extra detailed examinations and a clarification would be presented at the following section. Figure 3 indicates the remote phosphor structures with the flux of lamination which is depending on the current of the traditional and SiO_2 nanoparticles have a mass of 10 mg cm^{-2}. The CCT of 5010 and 5097 K at a driving current of 120 mA for both distant phosphorous structures as manufactured are almost the same. It is also evident that, at a motion stream of 120 mA, the luminous flux of the SiO_2 nano-particle configuration rises by 2.25%. The variation in refractive indices among interfaces could be minimized with SiO_2 nanoparticles layer, and the extraction of light can be improved. Since the SiO_2 nanoparticles refractive index has silicone is approximately 1.5 and the SiO_2 nanoparticles refractive index has silicone is around 1.8, the SiO_2 nanoparticles contain silicone can have a gradient refractive indices between the layers of phosphorus and air. So as to explain the role of the scattered influence of the differences of the CCT and the flux of lumination, the CCTs which has the dependent on angle of LED packs including distinct quantities of SiO_2 nanoparticles were examined and demonstrated in Figure 4. As the instruments were doped with SiO_2 nanoparticles, the consistency of the CCTs which has the dependent on angle was enhanced dramatically. This observation reveals that the growth of the dopant's SiO_2

nanoparticle concentration created a greater scattering impact. Generally, the CCTs consistency has the definition of the maximal CCT minus the minimal CCT. Left out doping with SiO2 nanoparticles, the correlation CCT was put at a great level (about 5319 K) and a greater CCT indicated a greater the light of blue extracted, which lead to an over CCT variance. The CCT differential found at 0° and 70° was effectively removed when the instruments were doped with SiO_2 nanoparticles. There was a clear impact of SiO_2 doping on phosphorus and silicone on the display of the packed equipment. However the optical features of SiO_2-doped films remain uncertain. In order to classify this combination of SiO_2-phosphor-silicone for further analysis, a sequence of thin-film experimentations were carried out, inclusive of transmitted absorption and haziness. At a wavelength of 460 nm compared to the normal dispensing configuration, the imbibition percentage in SiO_2 nanoparticle distributing configuration has been observed to rise from approximately 32% to almost 42%. This improvement resulted in the output of a greater portion of yellow light in the doped samplings of SiO_2, resulting in increasing the lighting performance. About this analysis, the effective index would change with the different SiO_2 nanoparticle concentrations after doping the SiO_2 nanoparticle in the phosphorus sheet. In comparison, the silicone, phosphorus and SiO_2 nanoparticle refractive indices (RI) are 1.4, 1.8 and 2.23. The RI of the SiO_2 nanoparticle phosphorous layer is then determined using the following equation [30]:

$$RI=V_1RI_1+V_2RI_2+V_3RI_3 \quad (15)$$

Where V_1, V_2 and V_3 are the concentrations of the materials, the weight ratio of the materials is measured. The combining ratio of the SiO_2 nanoparticles to the phosphorus substrate in the dispensing structure was 1 wt% and 3 wt% for the SiO_2 nanoparticle dispensing structure. Therefore the phosphor layer RIs is 1.428 and 1.445 in each layer. A TFCalc32 simulation was used to address the influence of the various refractive index layers. The light extraction for the SiO_2 nanoparticle dispensing structure is about the same relative to the traditional dispensing structure because of the almost equal refractive index. Therefore the improvement of SiO_2 nanoparticle dispensing structure lumen flux could be credited solely to the SiO_2 nanoparticle's dispersing impact. In order to numerical assess the scattered impact on the SiO_2 nanoparticles; a Mie-scatter reproduction was presented to investigate the scattered influences of the distinct SiO_2 impurity concentrations. There were no phosphors in our model and only SiO_2 nanoparticles in the medium were present to decrease the model's complexity. At a wavelength of 460 nm, the RI of the SiO_2 nanoparticle contain silicone was 2.23. The SiO_2 particle size was about 300 nm and the impurity content was roughly 1% and 3% for SiO_2 nanoparticles. As the wavelength was greater than 500 nm, the haze amplitude of the virtual system structure with a lower SiO_2 dopant content presented nearly 100% before hitting 500 nm and dropped steadily. The scattering effect of SiO_2 refers to our experimental results, according to the simulated results. The haze amplitude for doping with a higher SiO_2 material was about the same as for wavelengths ranging from 300 to 700 nm, see Figure 5.

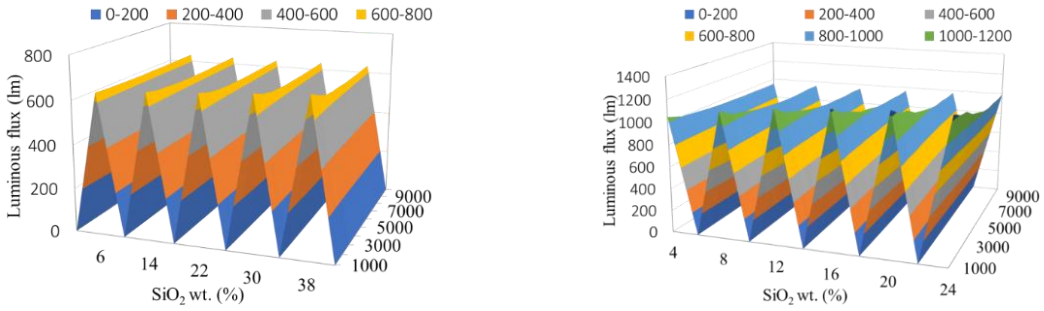

(a) (b)

Figure 5. Luminous fluxes of SiO_2 particles with different diameters, (a) Conformal structure, (b) In-cup geometry

The full-field finite-difference time-domain (FDTD) simulation is used to show the effect with the CCT consistency and luminous production with distinct SiO_2 nano-particle dimensions to examine the scattered strength which dependent on angle of various SiO_2 nano-particle dimensions for the light of blue and yellow. The refractive indices of SiO_2 nano-particles contain silicone is around 1.5 under the simulated

conditions, and the SiO_2 nano-particles' concentration is 5%. The SiO_2 nano-particles of 400 nm has been noted to have a higher scattered strength which dependent on angle than other dimensions in both incident lights of blue (450 nm) and yellow (560 nm), Figure 6. While the better scattering effect may result in great consistency of the CCT, the transmission of the light of blue and yellow in the usual way is important to consider. As the film develops thicker from our calculation of refined SiO_2/silicone film, we could view a stable increasing pattern of absorption. This absorption will make up for 5%-15% of light and should be greater as the nano-particle size becomes larger in the 300 nm SiO_2 particle example. Therefore in order to determine this condition, extensive absorption details of various nano-particle sizes are required, but it is sure that for dispersion purposes, the nano-particle size can not be increased indefinitely, see Figure 7.

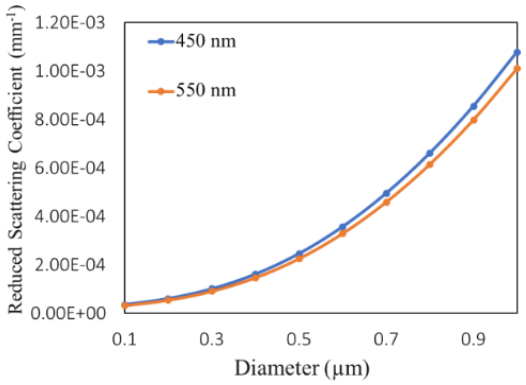

Figure 6. The reduced scattering coefficient of SiO_2 particles at different sizes and wavelength

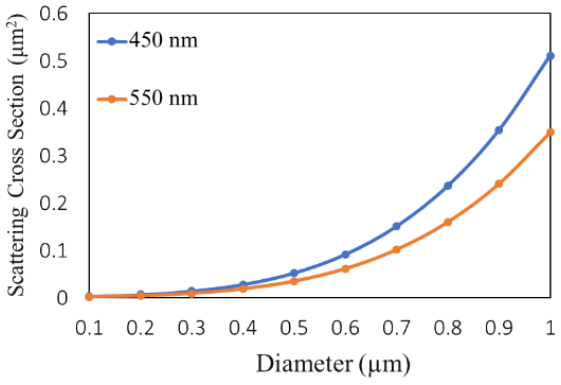

Figure 7. The scattering cross section of SiO_2 particles at different sizes and wavelength

The correlated strength which dependent on angle of the light of blue and yellow, is determined in order to examine how the scatter of nanoparticles determines the radiation of the in-cup phosphor form. The divergence angle of the light of blue is wider than that of the standard one in SiO_2 nano-particles with a remote phosphorous structure and blue light is diminished in the usual way. These phenomena suggest that the dispersion influence of SiO_2 nano-particles greatly affects the optic direction of the light of blue, which is leading to the increasing of CCT aberration; alternatively, the distribution of the yellow light of standard phosphorous structures and the distribution of SiO_2 nano-particles is approximately the same. This can be understood from the wavelength dependency of the haze ratio: the haziness of the 10 mg cm^{-2} sampling for yellow-colored photons (about 600 nm) is roughly 30% and 35% for blue-colored photons (about 450 nm). The larger the hazy scale, the higher the photon dispersion is. Correspondingly, blue photons are much more dispersed than yellow photons, which for SiO_2 samples on CCT may be helpful for color blending and cause less variance. This notion shows that the diffuse portion at wavelengths of yellow-colored light (600 nm) is a half of blue light and the haze calculation in Figure 5 also confirms this. These results indicate that in the distant phosphorus configuration, the CCT aberration is predominantly correlated with the divergence angle of the light of blue. In addition, the relative strength of blue light with distinct SiO_2 nano-particle weights at 700 was calculated as weight-dependent. Because of the maximum strength of the light of blue at broad angles, the SiO_2 nano-particle of 10 mg cm^{-2} is considered to have an optimized state.

4. CONCLUSIONS

In brief, we have incorporated nanocomposites with the base of SiO_2 accomodating CdSe-ZnS quantum dots at great concentrations through spray-diffusion of QDs and farther encapsulating by hydrolysis and condensation of TEOS. By the application of APS after spray-diffusion of QDs, the marked reduction in the strength of emissivity of nanocomposites after TEOS/ammonia insert to the SiO_2 layers was suppressed. Moreover, before spray processing, it was demonstrated the amount of QDs compounded into the nanocomposites was regulated by the insert of APS. In order to measure the effects of QD-SiO_2 nanocomposites on the radiation spectrum of white LEDs, we have created a white-emitting LED with QD-SiO_2 nanocomposites with a great load of QDs. The luminous performance of the QD-SiO_2 nanocomposite white LED was equivalent to that of the blue LED with the load of YAG:Ce and showed a great CRI and a little fall in lumination performance.

REFERENCES

[1] G. Zhang, K. Ding, G. He, and P. Zhong, "Spectral optimization of color temperature tunable white LEDs with red LEDs instead of phosphor for an excellent IES color fidelity index," *OSA Continuum*, vol. 2, no. 4, pp. 1056-1064, 2019, doi: 10.1364/OSAC.2.001056.

[2] K. Tsai, C. C. Cooksey, D. W. Allen, and C. C. White, "Exposure study on UV-induced degradation of PTFE and ceramic optical diffusers," *Applied Optics*, vol. 58, no. 5, pp. 1215-1222, 2019, doi: 10.1364/AO.58.001215.

[3] Q. Xu, L. Meng, and X. Wang, "Nanocrystal-filled polymer for improving angular color uniformity of phosphor-converted white LEDs," *Applied Optics*, vol. 58, no. 27, pp. 7649-7654, 2019, doi: 10.1364/AO.58.007649.

[4] T. DeLawyer, F. Rieke, and S. L. Buck., "Contrast-dependent red-green balance shifts depend on S-cone activity," *Journal of the Optical Society of America A*, vol. 35, pp. B114-B121, 2018, doi: 10.1364/JOSAA.35.00B136.

[5] R. Deshpande, A. S. Roberts, and S. I. Bozhevolnyi, "Plasmonic color printing based on third-order gap surface plasmons [Invited]," *Optical Materials Express*, vol. 9, no. 2, pp. 717-730, 2019, doi: 10.1364/OME.9.000717.

[6] L. Xu, B. Zhao, M. R. Luo, "Color gamut mapping between small and large color gamuts: part II. gamut extension," *Optics Express*, vol. 26, no. 13, pp. 17335-17349, 2018, doi: 10.1364/OE.26.017335.

[7] L. Duan, *et al.*, "Wide color gamut display w ith white and emerald backlighting," *Applied Optics*, vol. 57, no. 6, pp. 1338-1344, 2018, doi: 10.1364/AO.57.001338.

[8] L. V. Labunets, A. B. Borzov, and I. M. Akhmetov, "Regularized parametric model of the angular distribution of the brightness factor of a rough surface," *Journal of Optical Technology*, vol. 86, no. 10, pp. 618-626, 2019, doi: 10.1364/JOT.86.000618.

[9] L. Xiao, C. Zhang, P. Zhong, and G. He, "Spectral optimization of phosphor-coated white LED for road lighting based on the mesopic limited luminous efficacy and IES color fidelity index," *Applied Optics*, vol. 57, no. 4, pp. 931-936, 2018, doi: 10.1364/AO.57.000931.

[10] S. R. Chung, C. B. Siao, and K. W. Wang, "Full color display fabricated by CdSe bi-color quantum dots-based white light-emitting diodes," *Optical Materials Express*, vol. 8, no. 9, pp. 2677-2686, 2018, doi: 10.1364/OME.8.002677.

[11] K. Orzechowski, M. M. Sala-Tefelska, M. W. Sierakowski, T. R. Woliński, O. Strzeżysz, and P. Kula, "Optical properties of cubic blue phase liquid crystal in photonic microstructures," *Optics Express*, vol. 27, pp. 14270-14282, 2019, doi: 10.1364/OE.27.014270.

[12] A. D. Corbett, *et al.*, "Microscope calibration using laser written fluorescence," *Optics Express*, vol. 26, no. 17, pp. 21887-21899, 2018, doi: 10.1364/OE.26.021887.

[13] C. S. Kim, W. Kim, K. Lee, and H. Yoo, "High-speed color three-dimensional measurement based on parallel confocal detection with a focus tunable lens," *Optics Express*, vol. 27, no. 20, pp. 28466-28479, 2019, doi: 10.1364/OE.27.028466.

[14] S. Rasouli, S. Hamzeloui, and D. Hebri, "Colorful radial Talbot carpet at the transverse plane," *Optics Express*, vol. 27, no. 13, pp. 17435-17448, 2019, doi: 10.1364/OE.27.017435.

[15] A. Correia, P. Hanselaer, and Y. Meuret, "Holistic opto-thermal simulation framework for high-brightness light sources based on fluorescent conversion," *Optics Express*, vol. 27, no. 16, pp. A1324-A1337, 2019, doi: 10.1364/OE.27.0A1324.

[16] Lu, *et al.*,, "Synthesis and photoluminescence characteristics of the LiGd3 , MoO4.5:Eu3+ red phosphor with high color purity and brightness," *Optical Materials Express*, vol. 8, no. 2, pp. 259-269, 2018, doi: 10.1364/OME.8.000259.

[17] P. Zhu, H. Zhu, S. Thapa, and G. C. Adhikari, "Design rules for white light emitters with high light extraction efficiency," *Optics Express*, vol. 27, no. 16, pp. A1297-A1307, 2019, doi: 10.1364/OE.27.0A1297.

[18] Y. Li, Y. Wang, E. Y. B. Pun, and H. Lin, "Bead-on-string fibers electrospun from terbium acetylacetonate hydrate doped poly methyl methacrylate," *Optical Materials Express*, vol. 8, no. 2, pp. 276-288, 2018, doi: 10.1364/OME.8.000276.

[19] L. Wu, *et al.*, "Hybrid warm-white organic light-emitting device based on tandem structure," *Optics Express*, vol. 26, no. 26, pp. A996-A1006, 2018, doi: 10.1364/OE.26.00A996.

[20] J.i Chen, B. Fritz, G. Liang, X. Ding, U. Lemmer, and G. Gomard, "Microlens arrays with adjustable aspect ratio fabricated by electrowetting and their application to correlated color temperature tunable light-emitting diodes," *Optics Express*, vol. 27, no. 4, pp. A25-A38, 2019, doi: 10.1364/OE.27.000A25.

[21] J. Ruschel, *et al.*, "Current-induced degradation and lifetime prediction of 310 nm ultraviolet light-emitting diodes," *Photonics Research*, vol. 7, no. 7, pp. B36-B40, 2019, doi: 10.1364/PRJ.7.000B36.

[22] Z. Liu, *et al.*, "Effect of the replacement of Zn^{2+} with Mg^{2+} in $Ca_{14}Zn_6Ga_{10}O_{35}$:Mn^{4+}," *Optical Materials Express*, vol. 8, no. 9, pp. 2532-2541, 2018, doi: 10.1364/OME.8.002532.

[23] X. Wang, Y. Wang, J. Yu, Y. Bu, and X. Yan, "Modifying phase, shape and optical thermometry of NaGdF4:2%Er^{3+} phosphors through Ca^{2+} doping," *Optics Express*, vol. 26, no. 17, pp. 21950-21959, 2018, doi: 10.1364/OE.26.021950.

[24] Z. Huang, Q. Liu, M. R. Pointer, W. Chen, Y. Liu, and Y. Wang, "Color quality evaluation of Chinese bronzeware in typical museum lighting," *Journal of the Optical Society of America A*, vol. 37, no. 4, pp. A170-A180, 2020, doi: 10.1364/JOSAA.381498.

[25] G. Xia, Y. Ma, X. Chen, S. Q. Jin, and C. Huang, "Comparison of MAP method with classical methods for bandpass correction of white LED spectra," *Journal of the Optical Society of America A*, vol. 36, no. 5, pp. 751-758, 2019, doi: 10.1364/JOSAA.36.000751.

[26] C. Huang, Y. Chang, L. Han, F. Chen, S. Li, and J. Hong, "Bandwidth correction of spectral measurement based on Levenberg–Marquardt algorithm with improved Tikhonov regularization," *Applied Optics*, vol. 58, no. 9, pp. 2166-2173, 2019, doi: 10.1364/AO.58.002166.
[27] H. Daicho, K. Enomoto, H. Sawa, S. Matsuishi, and H. Hosono, "Improved color uniformity in white light-emitting diodes using newly developed phosphors," *Optics Express*, vol. 26, no. 19, pp. 24784-24791, 2018, doi: 10.1364/OE.26.024784.
[28] A. Krohn, G. J. M. Forkel, P. A. Hoeher and S. Pachnicke, "LCD-Based Optical Filtering Suitable for Non-Imaging Channel Decorrelation in VLC Applications," in *Journal of Lightwave Technology*, vol. 37, no. 23, pp. 5892-5898, 1 Dec.1, 2019, doi: 10.1109/JLT.2019.2941734.
[29] W. Zhong, J. Liu, D. Hua, S. Guo, K. Yan, and C. Zhang, "White LED light source radar system for multi-wavelength remote sensing measurement of atmospheric aerosols," *Applied Optics*, vol. 58, no. 31, pp. 8542-8548, 2019, doi: 10.1364/AO.58.008542.
[30] P. T. Tin, T. H. Q. Minh, N. H. K. Nhan, and H. Y, Lee, "Green-emitting CaF_2:Ce^{3+},Tb^{3+} phosphor: selection for improving luminous flux and color quality of conformal geometry white LED lamps." *Materials Science-Poland*, vol. 36, no. 4, pp. 563-569, 2018, doi: 10.2478/msp-2018-0095.